IEEE Access
Multidisciplinary | Rapid Review | Open Access Journal

Received September 4, 2019, accepted September 20, 2019, date of publication September 30, 2019,
date of current version October 10, 2019.

Digital Object Identifier 10.1109/ACCESS.2019.2944471

Beamsteering and Beamshaping Using a Linear Antenna Array Based on Particle Swarm Optimization

LUKASZ A. GREDA[1], (Senior Member, IEEE), ANDREAS WINTERSTEIN[1], (Member, IEEE), DANIEL L. LEMES[2], AND MARCOS V. T. HECKLER[2], (Member, IEEE)

[1]Institute of Communications and Navigation, German Aerospace Center (DLR), D-82234 Wessling, Germany
[2]Electromagnetics, Microwave and Antenna Laboratory, Universidade Federal do Pampa, Alegrete 97546-550, Brazil

Corresponding author: Lukasz A. Greda (lukasz.greda@dlr.de)

ABSTRACT This paper discusses the architecture of an adaptive transmitting microstrip array that allows highly flexible beamsteering and beamshaping. The antenna array is digitally controlled by a field programmable gate array (FPGA) board. The power and phase of the excitation signals delivered to the array elements are optimized using an algorithm based on particle swarm optimization (PSO), which includes all electromagnetic effects such as mutual coupling and installed performance. Further, the efficiency of the proposed approach is validated by synthesizing various beam patterns, including side lobe level control and beam shaping for cosecant squared and isoflux contours. Very good agreement between simulated and measured results is thereby observed. The paper also addresses implementation aspects that are not reported in detail in literature, such as the compensation for the faulty antennas or transmitting channels, as well as the calibration procedure applied for the experimental validation of the proposed architecture.

INDEX TERMS Active element pattern, beamforming, mutual coupling, optimization methods, particle swarm optimization, antenna measurement.

I. INTRODUCTION

The drastic increase in the number of wireless services in recent years has made it necessary to utilize the available spectrum in an efficient manner. Many users have to share the same frequency bands using space division multiple access (SDMA) techniques. The rational usage of spectrum and energy requires the radiated power to be concentrated to the maximum possible extent in the direction in which the microwave link is to be established. At the same time, radiation into other directions has to be minimized. In case of mobile terrestrial and satellite communications, the positions of the communication terminals are generally variable. In such cases, steerable antennas can be applied, which allow the radiation pattern of the antenna to be altered so as to maximize the signal-to-noise ratio or to minimize the power required to establish the communication link.

Adaptive antenna arrays allow the modification of the main beam by varying the amplitudes and phases of the signals that are delivered to the array elements [1]–[4]. If the desired pattern is not too complex, deterministic techniques may be used to estimate the amplitude and phase values. In such situations, the most popular methods are the renowned Dolph–Chebyschev distribution, the Woodward–Lawson method and the Fourier transform-based approaches [1]. However, in case of complex beam patterns, sophisticated heuristics have to be applied. This is due to the immense amount of possible combinations of amplitude and phase values which make a full search of the parameter space unfeasible. Therefore, some kind of optimization algorithm must be used to obtain a suitable excitation. Reviews of optimization methods can be found in [5] and [6]. The latter discusses the applications of optimization methods to various antenna problems. Particularly, the genetic algorithm (GA) and PSO have received considerable attention from the electromagnetics community. Both algorithms are evolutionary: GA is based on the natural evolution of species [7], whereas PSO is based on the dynamics and social interaction that can be observed among a swarm of bees [8]. An extensive comparison of these algorithms and

The associate editor coordinating the review of this manuscript and approving it for publication was Sotirios Goudos.

also modifications of them are reported in [9]. It is shown that the optimization results depend on the algorithm parameterization and the actual design problem. Therefore, no single algorithm is superior for all examples shown.

This work will focus on PSO as it allows global and local searches to be conducted simultaneously if the heuristic is set up in an appropriate manner. This is an advantage over GA. PSO is widely used to optimize antenna designs with respect to different performance metrics, e. g., reflection coefficient, cross-polarization or bandwidth [10]–[12].

Besides that, PSO also finds application in the optimization of antenna radiation patterns which is also the focus of this work. In [13] the authors demonstrate the use of PSO in the design of a communication antenna. Their optimization goals comprise reflection coefficient, gain and beamwidth of the radiation pattern. The paper does not detail which optimization criteria were used for the pattern. Optimization of beams of a reflectarray antenna was presented in [14]. For this, a mask with lower bounds for the main lobe and upper bounds for the sidelobes is used. The multibeam radiation pattern should fulfill the mask as closely as possible. The authors in [15] optimize the beam pattern of a synthetic aperture radar using a mask with upper and lower bounds. Simulated radiation patterns, noise equivalent sigma zero and range ambiguity-to-signal ratio curves are presented. These results show the improvement achieved by optimizing the array excitation coefficients.

Several studies to investigate adaptive antennas have been conducted based on the simplifications of the electromagnetic phenomena that cause reduction of the complexity of the required mathematical background. The typical approaches that are used include the usage of isotropic antennas and the absence of mutual coupling effects [16], [17]. In these cases, optimization is performed using only the array factor [18], [19]. However, as exhibited in [20], [21], the mutual coupling between the array elements cannot be ignored to obtain accurate results in case of realistic antennas. Additionally, the environment around the antenna may also influence the antenna performance [22]. Some other issues that have to be considered include the calibration inaccuracies [23], discretization of the excitation coefficients and, in some cases, antenna failure correction [24].

This paper reports an implementation of PSO that is used to perform beam pattern optimizations and takes the single element patterns, mutual coupling and installation platform effects into account. The cost function for the optimization is calculated using a novel mask technique. The desired pattern hereby has either to be above or below the mask or has to follow the mask as closely as possible. Introduced penalty weights specify the priorities in fulfilling the mask in certain regions if not all optimization goals can be fully achieved.

The performance of the presented optimization technique is demonstrated using mostly isoflux and cardioid shaped patterns. While many studies provide simulation results only, in this work the optimized excitation coefficients are validated by antenna measurements. Excellent agreement between predicted and observed results is thereby achieved. Furthermore, the robustness of the proposed array system was demonstrated by considering the failure of antennas in an array: because the antenna is fully adaptive, the beamforming coefficients can be recalculated if a failure is detected. Thus, it can ensure that the deviation of the impaired array pattern from the original one is as small as possible.

The proposed method can be applied to various satellite or terrestrial communication systems (e. g. 5G base stations). If only predefined patterns stored in a look-up table are used, it enables real-time operation with respond times of several milliseconds in case of digital beamforming.

The paper is organized as follows: Section II presents the optimization methodology, the mathematical background of PSO and its computational performance in comparison to other optimization techniques. Section III describes the design of the main radio frequency (RF) components and the digital hardware used for the experimental validation with an adaptive antenna array. In section IV, measurement results for several beam steering cases are given and compared to simulated data. Additionally, the optimization algorithm along with the integrated array are verified for the synthesis of radiation patterns with cosecant squared and isoflux-shaped beams. Thereby, very good agreement could be observed between the numerical and experimental results. Section V concludes the paper.

II. METHODOLOGY

A. BEAM SYNTHESIS

The performance of the presented optimization technique will be demonstrated using the following beamsteering and beamforming test cases that have high practical relevance:

1) steering the beam to 0°, 30° or 45° from broadside while controlling the sidelobe levels (SLL) within the positive hemisphere to −20 dB below the main beam level. Such a requirement must often be fulfilled to comply with regulations for transmission antenna or to minimize the interference in case of receiver antennas;
2) shaping the beam to obtain an isoflux pattern. This pattern can be used to reduce the required transmission power by delivering the same field strength in the served footprint of a satellite antenna;
3) shaping the beam to obtain a cosecant squared radiation pattern. This pattern can be used to deliver a constant field strength inside the coverage cell of a cellular base station;
4) compensation of a broken element for the beamsteering and beamshaping patterns.

The optimization problem that is considered in the study can be described as follows. An array of N antenna elements should be used to ensure that a given radiation pattern is synthesized as accurately as possible. Each antenna can be excited by an individual complex coefficient that represents the signal amplitude and phase. Without any loss of generality, normalizing the coefficient of an element in the array

TABLE 1. The penalty weights and behaviors of all the used masks. Where the regions are not mentioned, the masks have zero weight.

Pattern	region	w_m	b_m
Isoflux	$[-90, -50]$	1	-1
	$[-42, 42]$	2	0
	$[50, 90]$	1	-1
Cosecant squared	$[-90, 6]$	1	-1
	$[18, 75]$	2	0
0°, SLL = -20 dB	$[-90, -15]$	1	-1
	$[-14, 14]$	1	-1
	$[15, 90]$	1	-1
30°, SLL = -20 dB	$[-90, 14]$	1	-1
	$[15, 45]$	1	-1
	$[46, 90]$	1	-1
45°, SLL = -20 dB	$[-90, 22]$	1	-1
	$[23, 67]$	1	-1
	$[68, 90]$	1	-1

leads to $N-1$ degrees of freedom for the array excitation vector that can be denoted as $\mathbf{x} \in S$ where $S \in \mathbb{C}^{N-1}$ is the solution space. The objective of the optimization is to estimate an excitation vector $\hat{\mathbf{x}} \in S$ that can minimize the error between the synthesized and desired radiation patterns. This can be represented as

$$\min_{\mathbf{x}}\{F(\mathbf{x})\}, \quad \mathbf{x} \in S, \tag{1}$$

where $F(\mathbf{x})$ denotes the cost function that should be minimized to achieve optimization and where $F(\mathbf{x}) : \mathbb{C}^{N-1} \rightarrow \mathbb{R}_0^+$.

One of crucial parts of any optimization algorithm is the utilized cost function because it strongly influences the synthesis process and the synthesized pattern. In this work, a mask is used to describe the desired antenna array radiation pattern in the form of a normalized co-polarized electric field component $E_{\text{mask}}(\theta)$. In this work, only one-dimensional radiation patterns are considered. However, the presented method can be readily expanded to two-dimensional (2D) patterns as well.

To define the desired pattern behaviour for each test case a novel mask technique has been devised. Each mask can be divided into regions, in which the optimized pattern has to be below, above or exactly follow the mask. As fulfilling the mask criteria can generally have different priorities in different regions of the pattern, penalty weights for each region have been introduced. Table 1 shows the mask parameters for all the test cases shown in this paper.

The mask is evaluated at M discrete points of the angular range of the radiation pattern. A penalty weight $w_m \in \mathbb{R}_0^+$ and a behavior $b_m \in \{-1, 0, 1\}$, $m \in \{1, \ldots, M\}$ are assigned to each of these points. The values of b_m can be interpreted as follows:

- If $b_m = 0$, the pattern is expected to follow the mask as closely as possible. However, any deviation will increase the cost.
- If $b_m = +1$, the pattern is expected to stay above the mask. Undercutting the mask will again increase the cost.
- If $b_m = -1$, the pattern is expected to stay below the mask. Overshooting the mask will also increase the cost.

The cost function is formulated to sum the deviation between the mask and the array pattern that is obtained from a given excitation vector $\mathbf{x}$. The cost function can be given as

$$F(\mathbf{x}) = \sum_{m=1}^{M} w_m \frac{1}{1+|b_m|}\Big[\,\big|E_{\text{array}}(\mathbf{x}, \theta_m) - E_{\text{mask}}(\theta_m)\big| - b_m\left(E_{\text{array}}(\mathbf{x}, \theta_m) - E_{\text{mask}}(\theta_m)\right)\Big], \tag{2}$$

where E_{array} and E_{mask} are the magnitudes of the co–polarized field components in dB, normalized to pattern maximum. M is the number of angular points θ_m at which the cost function is evaluated.

B. PARTICLE SWARM OPTIMIZATION

The first work that investigated the application of PSO to problems in electromagnetics was [8]. The authors described PSO as "a robust stochastic evolutionary computation technique based on the movement and intelligence of swarms." In this work, PSO should be utilized to manipulate the magnitudes and phases of the antenna array excitation coefficients in order to obtain the desired radiation pattern.

In the majority of the practical problems a full search of all possible $\mathbf{x}$ in S is unfeasible even in case of small values of N. Therefore, PSO is used to obtained an optimized excitation vector with manageable computational effort. A flowchart of the PSO is exhibited in Fig. 1.

The algorithm begins with the creation of L random initial particles $\mathbf{x}_0^i, i \in \{1, \ldots, L\}$. Further, these particles are scattered over the entire solution space. At the beginning of each iteration, the cost function for every particle is evaluated. If a particle exhibits a lower cost than that exhibited by any other particle, it is stored as the current best global solution $\hat{\mathbf{x}}_{\text{g}}$. If the estimated cost of the current particle position is lower than that observed in all the previous iterations of a particle, the current position becomes the new personal best solution $\hat{\mathbf{x}}_{\text{p}}$.

The particles are supposed to move within the solution space from one iteration to the subsequent iteration. Therefore, each particle exhibits a velocity of $\mathbf{v}_k^i \in \mathbb{C}^{N-1}$. Further, the initial velocity vectors $\mathbf{v_0^i}$ are drawn in a random manner. After evaluating of the cost function of each particle, its velocity can be given as

$$\mathbf{v}_{k+1}^i = c_0 \cdot \mathbf{v}_k^i + c_1\eta_1(\hat{\mathbf{x}}_{\text{p}} - \mathbf{x}_k) + c_2\eta_2(\hat{\mathbf{x}}_{\text{g}} - \mathbf{x}_k), \tag{3}$$

where c_0 can be interpreted as the inertia of the particle, while c_1 and c_2 determine the manner in which the particle is influenced by the global and personal best. The range of these parameters is $c_0, c_1, c_2 \in [0, 1]$ [8]. In this study, $c_0 = 0.9$ and $c_1 = c_2 = 1.5$ are set for all the optimizations. The variables η_1 and η_2 are random variables that are drawn from

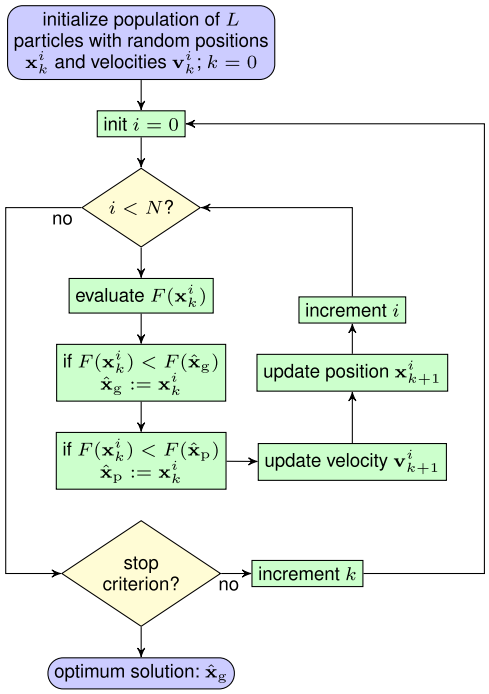

FIGURE 1. Flowchart of PSO, which is modified from [8].

a uniform distribution according to

$$\eta_1, \eta_2 \sim \mathcal{U}(0, 1). \tag{4}$$

Finally, the particle positions in the solution space are updated according to

$$\mathbf{x}_{k+1}^i = \mathbf{x}_k^i + \mathbf{v}_k^i \cdot \Delta t, \tag{5}$$

where Δt denotes the dimensionless step size of the algorithm. For the optimizations that are presented in this paper $\Delta t = 1$.

As long as the stopping criteria of the algorithm are not satisfied, a new iteration is initiated, i.e., k is incremented. As stopping criteria, a maximum number of iterations or a certain value that should be achieved by the cost function may be chosen.

C. COMPARISON WITH OTHER OPTIMIZATION TECHNIQUES

Performance of PSO was compared to two other global optimization techniques - Taguchi's method and firefly algorithm.

Taguchi's method is a global optimization technique that applies a concept of orthogonal array to reduce number of tests required in an optimization process. It was introduced to electromagnetic simulations by [25] and the formulation proposed there was implemented in this study for performance comparison. In contrast to PSO, in Taguchi's method no random values are used and therefore this technique leads to exactly the same optimization results for each run. A performance comparison and integration of Taguchi's method and PSO was described in [26].

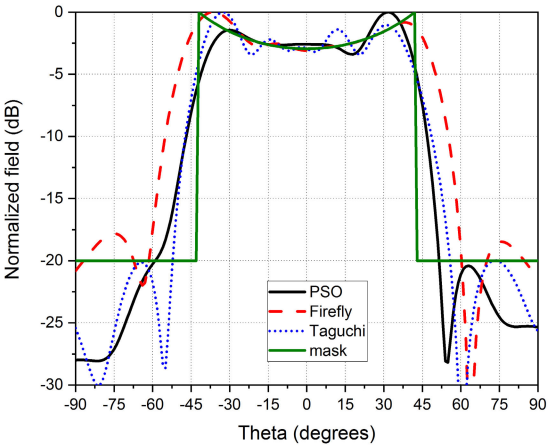

FIGURE 2. A comparison between the optimized patterns using PSO, firefly and Taguchi's method.

The firefly algorithm (FA) is another nature inspired heuristic, which has been first introduced in 2009 [27]. It is based on the behavior of fireflies, whereby the bioluminescence is used to attract partners for mating. The attraction is weighted by the bioluminescence intensity, which depends on how close the fireflies are to the optimal solution, and by the distance between the fireflies.

For performance comparison between PSO, Taguchi's method and FA, simulated radiation patterns of the 8×1 patch array described in Sec. III-A were used. Fig. 2 shows the optimized patterns for the isoflux mask described in Table 1.

The residual cost functions calculated for this case using (2) are: PSO 152.0, Taguchi's method 166.5, FA 259.4. The optimization times using Matlab codes were (in seconds): PSO 31.7, Taguchi's method 194.8 and FA 55.4. Also for several other cases not shown in this study, the performance of PSO was at least slightly better and optimization time shorter than for the both other algorithms.

III. EXPERIMENTAL SETUP

To assess the beamforming potential of PSO in case of realistic antenna arrays, the transmitter (Tx) path of the retro-directive antenna demonstrator that was presented in [28] was used. In the subsequent section, a description of the relevant parts of the system is provided. Additionally, the necessary calibration procedure and the measurement setup in a compact test range (CTR) are described.

A. HARDWARE COMPONENTS

The antenna array is a linearly polarized 8×1 patch array that resonates at 7.0 GHz. The distance between the elements is half of the free space wavelength. The antenna comprises the following two substrate layers: Rogers RO4003 with a thickness of 1.524 mm for the upper substrate and Rogers RO3206 with a thickness of 0.635 mm for the lower substrate. Both the substrates exhibited dimensions of 21.4 $\times$ 8.5 cm and were connected using Rogers RO4403 prepreg with a height of 0.2 mm. As radiating element rectangular patch

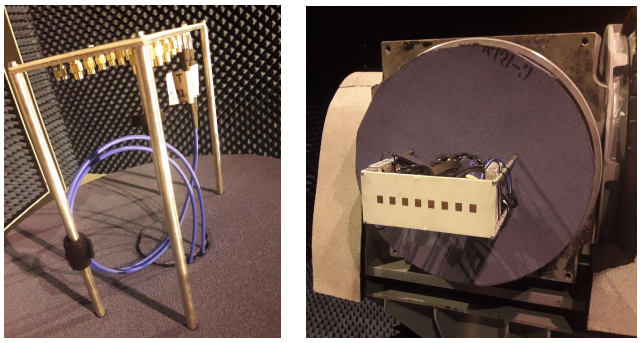

(a) (b)

FIGURE 3. Schematics of the measured passive antenna in a compact test range. (a) A setup to measure the embedded patterns. (b) A setup to measure the radiation pattern of the whole array.

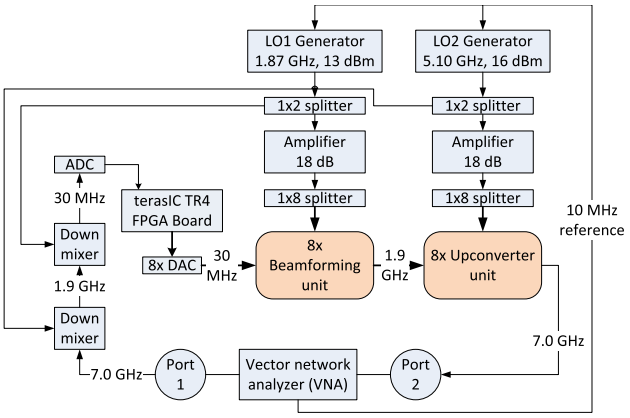

FIGURE 4. Setup to calibrate all eight transmitter front-ends including the digital hardware.

having dimensions of 10.1 × 12.5 mm is used. The patches are fed by vias (each having a diameter of 0.8 mm) that were connected to the feed lines located on the lower side of the upper substrate. Fig. 3 schematically depicts the passive array that is mounted on a positioner in the CTR.

The antenna ports are connected to the transmitter front-ends with analog beamforming capability. A detailed description of these front-ends can be observed in [29]. They comprise two up-converter stages. In the first stage, the front-end input signal is up-converted to an intermediate frequency (IF) of 1.9 GHz. Further, analog beamforming capability is demonstrated on this IF with a digitally controlled phase shifter and a variable gain amplifier (VGA). During the second stage, the IF signal is mixed up to 7.0 GHz and is fed to the antenna array. The overall gain of the front-ends is observed to be approximately 10.0 dB. Further, the VGAs and phase shifters were both controlled by 6 bit words. Therefore, 64 different states are possible which theoretically allows controlling the phase in steps of 5.6°. In this work, the analog beamforming capability of the front-ends was used only to perform calibration, i.e., to equalize the phase and amplitude differences between all eight Tx channels.

To ensure that maximum flexibility can be obtained, digital beamforming was conducted using a FPGA. An analog input signal was digitized and processed by a Hilbert filter to ensure that a complex representation of the input signal can be obtained. This signal was further multiplied with eight complex coefficients which created the weighted signals that were required for beamforming. These eight signals were delivered to the digital-to-analog converters (DACs), which were connected to the transmitter front-end inputs.

B. CALIBRATION PROCEDURE

Calibrating the individual transmission channels is a major requirement for successful beamshaping. The objective of the calibration is to ensure that a single input signal delivered to the system arrives with equal magnitude and phase at each antenna port. The laboratory setup that is used to achieve calibration is depicted in Fig. 4. The eight transmitter front-ends are exhibited in the center of the diagram. Each of the front-ends comprise a beamforming and an upconverter unit. Further, two signal generators were used to obtain the necessary local oscillator (LO) signals at 1.87 and 5.1 GHz. After a 1 × 2 splitter, each LO signal was amplified and distributed to the eight front-ends using 1 × 8 splitters.

A vector network analyzer (VNA) was used to perform the calibration measurements. Its reference output of 10 MHz ensured that all the devices in the setup were appropriately synchronized. The VNA was set to measure the S-parameters around 7.0 GHz which was the desired output frequency of the transmitter front-ends. The VNA signal from port 1 was further used as input for the transmitter system. The VNA signal was down-converted in two stages to a frequency of 30 MHz whereby the same LO signals as for the front-ends were used. Further, the down-converted signal was sampled by an analog-to-digital converter (ADC) and was fed to the FPGA. To achieve calibration, the digital beamforming was deactivated, i.e., all the weights were set to 1.0. Thus, the FPGA created eight identical output signals which were D/A converted and put out to the eight front-ends.

Calibration was achieved by successively connecting each of the eight front-end outputs to the VNA and by adjusting the setting of the respective phase shifter and VGA. Fig. 5a exhibits the front-ends during calibration. It can be observed that the front-ends were disconnected from the antenna array while performing the measurements. The described setup allows the calibration of the complete analog and digital signal paths. Furthermore, calibration can also be achieved by performing a regular VNA S-parameter measurement. No vector mixer measurements are necessary because there is no requirement to measure the absolute gain of the system, due to the fact that only the equalization of the relative differences between the channels has to be achieved.

Because the calibration was performed using digitally-controlled phase shifters and VGAs, only discrete values

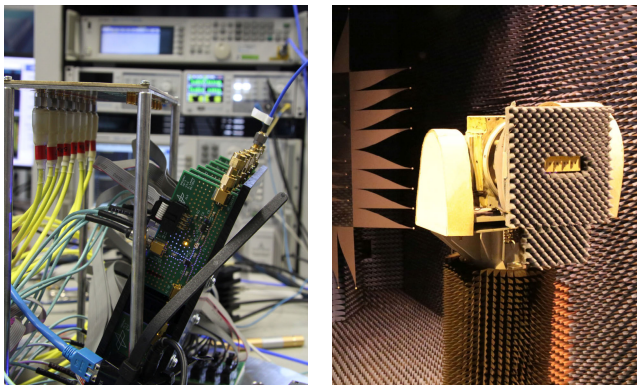

(a) (b)

FIGURE 5. Schematics of the measured active antenna. (a) Antenna array with disconnected front-ends for calibration. During operation, the front-ends are directly screwed on the antenna with SMA connectors. (b) Active antenna with absorbers covering the additional hardware.

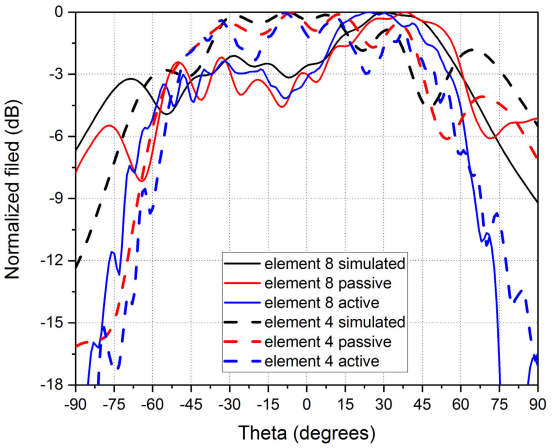

FIGURE 6. A comparison of embedded element patterns for two elements (edge and middle one) of the 8 × 1 array.

could be set. This resulted in amplitude standard deviation of 0.38 dB and phase standard deviation of 3.7° between the front-ends after calibration.

C. MEASUREMENT SETUP

After achieving calibration, the transmitter system was installed in the CTR. The measurement setup was similar to the one depicted in Fig. 4 with the following exceptions:

1) The outputs of the eight upconverter units were connected to the antenna array;
2) Port 2 of the VNA was connected to the measurement antenna of the CTR;
3) Measurement signals were transmitted between the antennas.

A photograph of the antenna array on the positioner is provided in Fig. 5b. The radio-frequency absorbers were used to cover the FPGA, splitters, and amplifiers that were also mounted on the positioner. Further, the signal generators and down mixers were located at the base of the positioner. The phase shifters and VGAs of the front-ends were loaded with the values that were determined during calibration. For beam steering and beamshaping, the digital beamforming within the FPGA was used.

IV. RESULTS

The performed investigations include the influence of the element patterns that are used for optimizations, the influence of the discretization of magnitude and phase of excitation coefficients, and the compensation of the faulty elements. To perform comparison between different patterns that are used for optimization, the isoflux and cosecant masks are selected in a manner that they cannot be completely satisfied with the array (i.e., the cost function is always higher than zero). All the diagrams shown in the subsequent sections have been optimized and plotted for the co-polarized electric field component.

A. INFLUENCE OF THE EMBEDDED PATTERNS FOR OPTIMIZATION

To examine the influence of the element patterns that are used in PSO on the measured results, the following three cases have been investigated.

a: ISOTROPIC

an array of ideal isotropic antennas was considered. Therefore, element patterns, mutual coupling, and installed performance were not taken into account.

b: PASSIVE

the measured radiation patterns of the passive antenna array were used, i.e., only the passive array without RF electronics. The patterns were measured one after the other, and all the non-active elements terminated with 50 Ω. All the patterns were stored with an angular resolution of 1°. Fig. 3 depicts the passive antenna that is mounted on the positioner in the CTR.

c: ACTIVE

the embedded element patterns were measured in a manner similar to that used for the passive case, but now with the full Tx system integrated. Fig. 5b depicts the active antenna that is mounted on the positioner in the CTR. The front-ends and other electronic components were hidden behind the RF absorbers to minimize their influence on the antenna.

Fig. 6 depicts a comparison of the simulated and measured embedded radiation patterns in passive and active environments in the steering plane for two array elements (one middle element and one edge element). As can be observed, there is a significant difference between the patterns for an edge element and middle element due to mutual coupling. Further, the results for the same element obtained by full-wave simulations with the commercial electromagnetic field simulation software ANSYS HFSS and by the measurements in passive and active configurations are observed to differ.

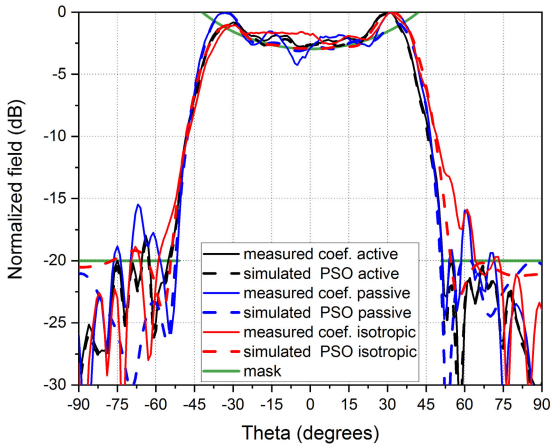

FIGURE 7. A comparison between the optimized results obtained with active patterns, passive patterns, and isotropic elements for an isoflux shape.

This difference is generally observed to increase towards the horizon. The main reason for this behavior is the existence of specular reflections and diffraction of the platform on which the array has been mounted and which are different while performing passive and active measurements; further, the specular reflections and diffraction of the platform are not considered during HFSS simulations. Additionally, each element was fed with identical values of power in case of passive antenna measurements. In case of active antenna measurements, the delivered power for each antenna element varied with an amplitude standard deviation of 0.38 dB because of the imperfections in the RF front–end calibration with analog components (see Sec. III-B). Therefore, each antenna element contributes to the overall radiation pattern with a slightly different power factor. All these effects result in standard deviation radiation pattern amplitude variations at a boresight of 0.23 dB in case of the passive array and at 1.21 dB in case of the active array. The higher value for the active array can be attributed to the influence of front-ends and the coupling with the electronics behind the antenna.

To demonstrate how the use of active and passive measured patterns with PSO influences the measured results, an isoflux-shaped pattern with specifications as shown in Table 1 has been synthesized. Initially, PSO has been run with the elemental patterns measured in passive mode to obtain the array excitation vector. In a further step, PSO has been run with the elemental patterns measured in active mode. For the sake of comparison, the same procedure has been carried out for an array of isotropic elements. These three array excitation vectors have been used to excite the array in the CTR and the results are shown in Fig. 7, where the mask is shown in green. Since the cost function is a measure of how the pattern deviates from the desired mask, it can be used to compare the quality of the patterns. The residual cost function values for all the cases are presented in Table 2. The smallest value is obtained for beamforming coefficients that are computed using the active element patterns. This value is

TABLE 2. Values of the residual cost function using the PSO algorithm in case of the isoflux and cosecant masks.

Scenario	Isotropic		Passive		Active	
	sim.	meas.	sim.	meas.	sim.	meas.
Isoflux	127.0	261.9	91.7	186.3	150.3	172.2
Cosecant squared	51.3	221.7	55.4	364.8	63.6	78.7

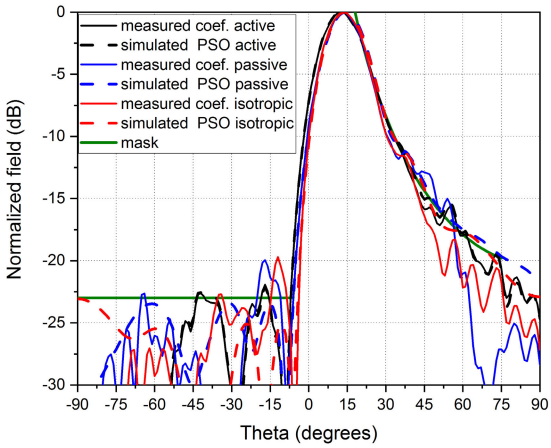

FIGURE 8. A comparison between the optimized results obtained with active patterns, passive patterns, and isotropic elements for a cosecant squared shape.

similar to that obtained with the PSO code at the end of the optimization process. The pattern measured with the coefficients computed using the passive patterns yielded larger cost because the platform-installed performance and the influence of the front-ends were not considered during optimization. The largest deviation from the mask was observed for the pattern measured by using the coefficients optimized using isotropic elements. In this case, mutual coupling and platform effects were not considered.

The synthesis of a cosecant squared shaped pattern has been also considered by using the same procedure described above. The pattern specifications are described in Table 1. The resulting patterns are shown in Fig. 8 and the values of the residual cost function are displayed in Table 2. Similar behavior can be observed, since the curve measured using the coefficients obtained with active element patterns is the one that best satisfies the cosecant squared mask. It should be highlighted that very good representation of the mask has been achieved by using the active elemental patterns during the optimizations run with PSO and that excellent agreement between the calculated and measured patterns have been obtained.

B. STEERING PROPERTIES AND SIDELOBE LEVEL CONTROL

The ability to achieve nearly arbitrary beamshapes can also be used to perform accurate beam steering with simultaneous sidelobe level suppression. As mentioned above, mutual coupling, installed performance and inaccuracies in front-end calibration influence the actual amplitude and phase values

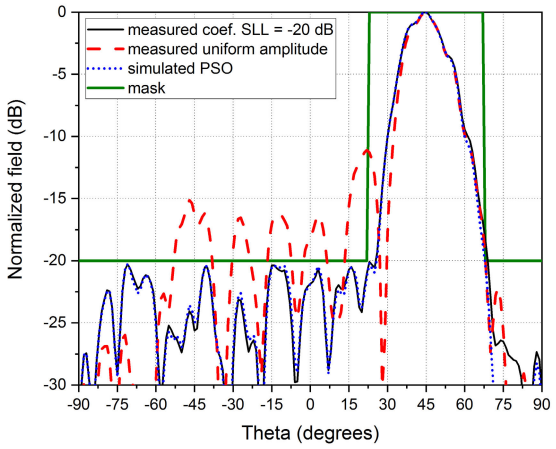

FIGURE 9. A comparison between the patterns with and without control of SLL for steering to 45°.

that are required to obtain a desired array radiation pattern. If these effects are not considered, which is the case while using simple deterministic beamsteering or beamforming algorithms with isotropic elements, the resulting amplitude and phase values cause deviations in the generated radiation pattern. As described in [4], the influence of amplitude and phase errors on the radiation pattern of array antennas can be approximated using the following expressions:

$$\frac{G}{G_0} \approx \frac{1}{1+\sigma^2} \tag{6}$$

$$\mathrm{SLL} = \mathrm{SLL}_0\sqrt{1+\sigma^2/(G_0 \cdot \mathrm{SLL}_0^2)} \tag{7}$$

$$\sigma^2 = (\sigma_a - 1)^2 + \sigma_\phi^2 \tag{8}$$

where G_0 is the error-free directivity, SLL_0 is the design sidelobe level, σ_a is the amplitude standard deviation and σ_ϕ is the phase standard deviation, in radians.

Further, the standard deviation of the beam pointing error for an uniform linear array normalized to the 3-dB beamwidth θ_3 is [4]

$$\frac{\sigma_\theta}{\theta_3} = \frac{0.622\sigma}{\sqrt{N}} \tag{9}$$

where N is the number of elements.

For the designed active array, the amplitude standard deviation is $\sigma_a = 1.21\ dB$ (1.15), whereas the phase standard deviation $\sigma_\phi = 5.58°$ (0.097). This results in a gain reduction of 0.13 dB and standard deviation of the beam pointing error of 0.55° if excitation coefficients for an isotropic array are used.

Fig. 9 depicts a comparison between the measured radiation patterns steered to 45° with an SLL suppression of −20 dB using PSO (for mask details, see Table 1) and using the simple progressive phase shift that is calculated for the isotropic elements. The sidelobe level obtained using simple beam steering is −11.10 dB, which is greater than the theoretical value of −12.8 dB for isotropic radiators. The measured sidelobe level increase is due to influence of active element patterns slightly higher than the theoretical sidelobe level increase that is calculated using (7) for isotropic radiators, which is observed to be 0.32 dB. In both the cases, the maximum radiation was attained for the desired steering angle.

TABLE 3. Main beam squint due to element patterns for high steering angles in case of steering coefficients calculated with isotropic elements.

desired steering angle	60°	65°	70°	75°	80°	85°
achieved steering angle	58°	63°	66°	69°	71°	73°
beam deviation error	2°	2°	4°	6°	9°	12°

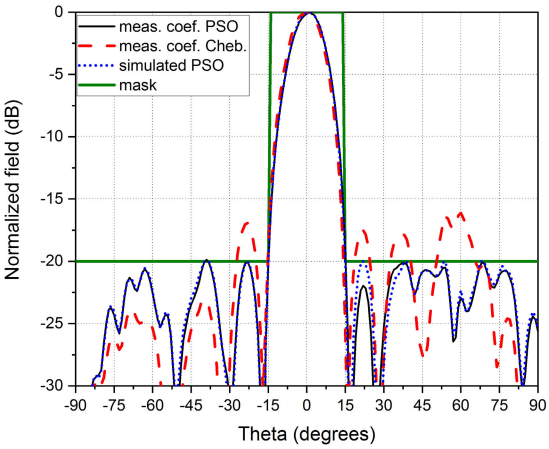

FIGURE 10. A comparison between PSO and Dolph–Chebyshev for steering to a boresight and for an SLL control of −20 dB.

However, a main beam squint due to element pattern was observed to occur for steering with coefficients that were calculated in case of isotropic arrays for large steering angles. Table 3 presents the main beam squint of the measured antenna for some sample steering angles. The PSO algorithm compensates for the influence of element patterns and therefore delivers an accurate steering angle in the whole steering region of the array.

Fig. 10 depicts a comparison between the two radiation patterns that were measured with the coefficients obtained by PSO and the Dolph–Chebyshev algorithm. The selected mask is described in Table 1. The objective of both the algorithms was to reduce the sidelobe levels to at least 20 dB below the main lobe level. PSO could successfully complete this task by working with the active measured element patterns to optimize the antenna coefficients. However, the sidelobe levels that were measured with the coefficients calculated using the Dolph–Chebyshev algorithm were significantly higher than the mask in some regions, since this approach does not take the effects of mutual coupling into account. Also in this case the measured increase in the SLL is slightly higher than the theoretical one that was calculated using (7), which is observed to be 1.5 dB.

C. INFLUENCE OF DISCRETIZATION

The optimized beamforming coefficients for all the measurements that have been performed in this study are set in the

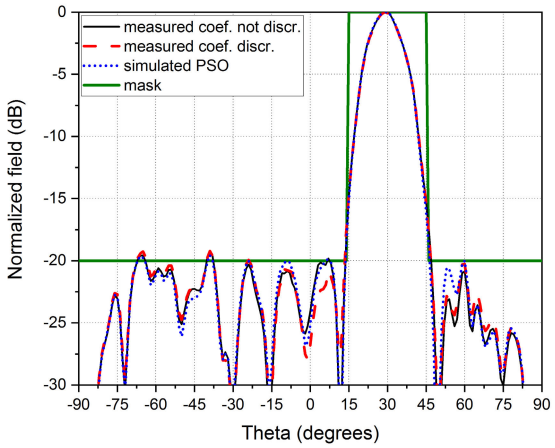

FIGURE 11. The influence of discretization on the optimized radiation pattern for steering to 30° and for an SLL control of −20 dB.

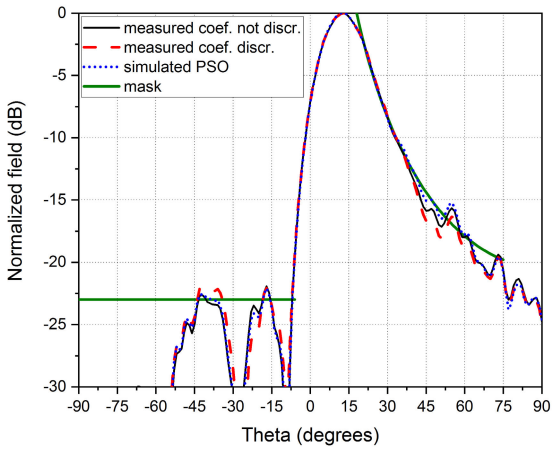

FIGURE 12. The influence of discretization on the optimized radiation pattern for a cosecant squared shape.

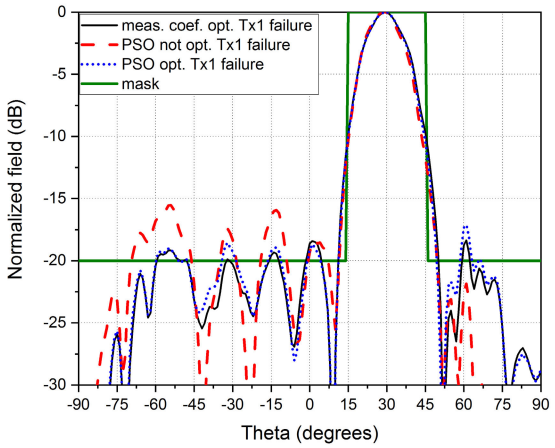

FIGURE 13. A compensation of the broken element Tx1 for beam steering to 30° and an SLL control of −20 dB.

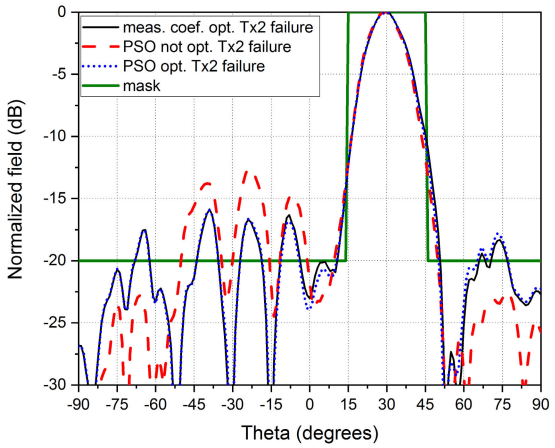

FIGURE 14. A compensation of the broken element Tx2 for beam steering to 30° and an SLL control of −20 dB.

digital domain. However, the front-ends that were used in the measured system enabled beamforming in the analog domain using VGAs and phase shifters as described in Sec. III-B. The analog components were digitally controlled by 6-bit words so that only discrete values can be set. Through discretization, additional amplitude and phase errors are introduced.

The influence of discretization on the performance of the measured results was examined for several cases with active element patterns. Fig. 11 depicts a comparison between optimized radiation patterns for steering the main lobe to 30° and sidelobe level control of −20 dB. In this case, the theoretical directivity is reduced by only 0.014 dB, the SLL increases by 0.17 dB, and a beam pointing error occurs with a standard deviation of 0.18°, since $\sigma_a = 0.25\ dB$ (1.029) and $\sigma_\phi = 2.81°(0.049\ rad)$.

Fig. 12 shows a comparison for the cosecant squared shape.

The increase in SLL for the cosecant squared shape and SLL of −23 dB is 0.34 dB. The discrepancies between the patterns that were obtained with and without discretization of the coefficients were insignificant in both cases. Further, for other measured cases that are not provided in this paper, the discrepancies are observed to be marginal. Therefore, digitization of the excitation coefficients with 6 bits exhibits only negligible negative impact in case of the proposed architecture.

D. COMPENSATION OF BROKEN ELEMENTS

If one of the array elements does not work properly (e. g., due to failure of an amplifier), the radiation pattern of the array changes, which will mostly result in diminished gain and higher sidelobe levels. This can also cause the violation of a regulatory mask in case of transmission antennas or a decrease in the signal-to-noise ratio in case of receiver antennas. However, it is possible to minimize these negative effects using a suitable optimization algorithm. To examine the capability of the proposed approach to compensate for one faulty element, two cases were chosen: steering to 30° with an SLL control of −20 dB and shaping the beam to a cosecant squared. For both these cases, the first four elements of the transmission arrays were successively set as off. Figs. 13 and 14 exhibit comparisons between the results that

TABLE 4. Values of the residual cost function for steering to 30° and cosecant squared shape.

Scenario	Simulated initial	Simulated optim.	Measured optim.
30°, SLL = -20 dB, all active	–	4.0	7.1
30°, SLL = -20 dB, Tx1 failure	137.8	64.7	60.6
30°, SLL = -20 dB, Tx2 failure	213.6	114.0	115.4
30°, SLL = -20 dB, Tx3 failure	269.6	189.2	195.9
30°, SLL = -20 dB, Tx4 failure	564.7	494.9	497.9
Cosecant squared, all active	–	63.6	78.7
Cosecant squared, Tx1 failure	114.9	78.8	–
Cosecant squared, Tx2 failure	262.4	116.3	124.7
Cosecant squared, Tx3 failure	323.1	164.6	175.9
Cosecant squared, Tx4 failure	920.0	332.1	352.0

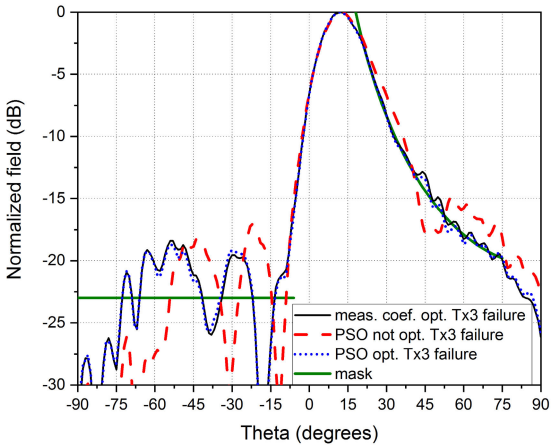

FIGURE 15. A compensation of the broken element Tx3 for a cosecant squared shape.

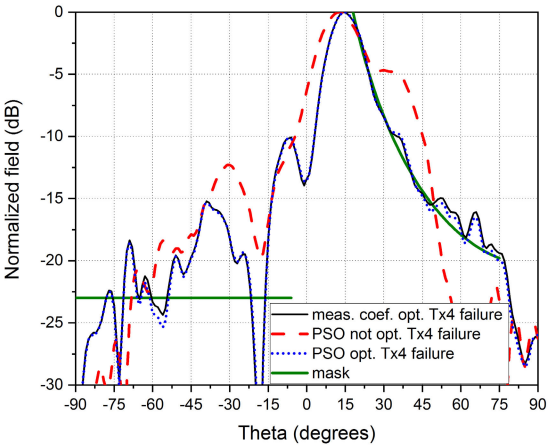

FIGURE 16. A compensation of the broken element Tx4 for a cosecant squared shape.

are obtained after failure of Tx elements 1 and 2, respectively, prior to and after new optimization of the excitation coefficients, so as to compensate for the loss of an array element. As observed in the previously depicted cases, a very good agreement was achieved between the measured and simulated results. The improvement in terms of the residual cost function that is computed using (2) is exhibited for the Tx elements 1–4 in Table 4. As can be observed, the cost function is generally greater for elements that are close to the center of the array. In all the cases the radiation patterns can be significantly improved (i.e., the cost function can be minimized) if PSO considers the element failure.

A very similar behavior can be observed in case of the patterns having a cosecant squared shape. Figs. 15 and 16 exhibit the corresponding cases for failures in the array elements 3 and 4. For optimizations of the cosecant squared shape, the left part of the mask, which was used to control the sidelobe level, exhibited twice as low priority as compared to that exhibited by the right part with the actual cosecant squared shape (see Table 1). Therefore, there is only a slight improvement in the level of sidelobes between the compensated and the non-compensated cases. However, there is a significant improvement that is observed in the cosecant squared shape. The optimized curved can follow the cosecant squared shape with much smaller deviations. Table 4 presents the values of cost function for the Tx elements 1–4. One measurement with the broken element 1 is missing, because erroneous excitation coefficients were loaded for this case. As for the beamsteering scenario, the cost function increases when the broken element is located closer to the array center. By performing PSO optimizations after element failure, the cost function could be minimized, hence yielding radiation patterns significantly improved.

V. CONCLUSION

This paper presented a method using PSO to obtain nearly arbitrary beam shapes with a transmitting microstrip array. Further, a mathematical description of PSO was introduced and adopted to solve the problem of radiation pattern shaping using a pattern mask. An experimental setup was developed to validate the performance of the beamshaping. The developed setup contained both analog and digital beamforming capabilities; the former was used for calibration, whereas the latter was employed to excite the array in accordance with the PSO result. Special attention was devoted to the calibration procedure of the system and the measurement setup in the CTR.

The performance of the PSO was evaluated using isotropic, simulated, and measured single element patterns for optimization. It was observed that the antenna array pattern synthesis can deliver very accurate results using PSO. As can be expected, the congruence between the predicted and measured radiation patterns was excellent or very good, especially when the element patterns and platform effects were completely considered. The beamshaping results were presented for isoflux and cosecant squared shaped beams. Additionally, the ability to significantly suppress the sidelobes was demonstrated. Further, the influence of discrete steps in the beamforming coefficients on the beamshaping results was also analyzed. Finally, the potential improvement of the per-

formance in case of the failure of an antenna element was exhibited.

The applicability of PSO to array beam pattern shaping was proved based on the practical demonstrations presented in this paper. This method is suitable to enhance the performance of transmission systems with analog or digital beamforming and demands low computational resources.

ACKNOWLEDGMENT

The authors would like to thank Georg Buchner and Wahid Elmarissi for their help in building the experimental antenna system, Bernd Gabler for fruitful discussions on measurement setup and performing the measurements in the CTR, and Eduardo Yoshimoto for the results generated with the firefly algorithm.

REFERENCES

[1] C. A. Balanis, *Modern Antenna Handbook*. Hoboken, NJ, USA: Wiley, 2007.
[2] H. J. Visser, *Array and Phased Array Antenna Basics*. Hoboken, NJ, USA: Wiley, 2006.
[3] A. J. Fenn, *Adaptive Antennas and Phased Arrays for Radar and Communications*. Norwood, MA, USA: Artech House, 2007.
[4] R. C. Hansen, *Phased Array Antennas*. Hoboken, NJ, USA: Wiley, 1998.
[5] J. W. Bandler, "Optimization methods for computer-aided design," *IEEE Trans. Microw. Theory Techn.*, vol. MTT-17, no. 8, pp. 533–552, Aug. 1969.
[6] S. H. Yeung, W. S. Chan, K. T. Ng, and K. F. Man, "Computational optimization algorithms for antennas and RF/microwave circuit designs: An overview," *IEEE Trans. Ind. Informat.*, vol. 8, no. 2, pp. 216–227, May 2012.
[7] F. J. Ares-Pena, J. A. Rodriguez-Gonzalez, E. Villanueva-Lopez, and S. R. Rengarajan, "Genetic algorithms in the design and optimization of antenna array patterns," *IEEE Trans. Antennas Propag.*, vol. 47, no. 3, pp. 506–510, Mar. 1999.
[8] J. Robinson and Y. Rahmat-Samii, "Particle swarm optimization in electromagnetics," *IEEE Trans. Antennas Propag.*, vol. 52, no. 2, pp. 397–407, Feb. 2004.
[9] A. Deb, J. S. Roy, and B. Gupta, "Performance comparison of differential evolution, particle swarm optimization and genetic algorithm in the design of circularly polarized microstrip antennas," *IEEE Trans. Antennas Propag.*, vol. 62, no. 8, pp. 3920–3928, Aug. 2014.
[10] H. Wu, J. Geng, R. Jin, J. Qiu, W. Liu, J. Chen, and S. Liu, "An improved comprehensive learning particle swarm optimization and its application to the semiautomatic design of antennas," *IEEE Trans. Antennas Propag.*, vol. 57, no. 10, pp. 3018–3028, Oct. 2009.
[11] S. Chamaani, S. A. Mirtaheri, and M. S. Abrishamian, "Improvement of time and frequency domain performance of antipodal vivaldi antenna using multi-objective particle swarm optimization," *IEEE Trans. Antennas Propag.*, vol. 59, no. 5, pp. 1738–1742, May 2011.
[12] E. J. B. Rodrigues, H. W. C. Lins, and A. G. D'Assunção, "Fast and accurate synthesis of electronically reconfigurable annular ring monopole antennas using particle swarm optimisation and artificial bee colony algorithms," *IET Microw., Antennas Propag.*, vol. 10, no. 4, pp. 362–369, 2016.
[13] A. A. Minasian and T. S. Bird, "Particle swarm optimization of microstrip antennas for wireless communication systems," *IEEE Trans. Antennas Propag.*, vol. 61, no. 12, pp. 6214–6217, Dec. 2013.
[14] P. Nayeri, F. Yang, and A. Z. Elsherbeni, "Design of single-feed reflectarray antennas with asymmetric multiple beams using the particle swarm optimization method," *IEEE Trans. Antennas Propag.*, vol. 61, no. 9, pp. 4598–4605, Sep. 2013.
[15] R. Zhou, J. Sun, S. Wei, and J. Wang, "Synthesis of conformal array antenna for hypersonic platform SAR using modified particle swarm optimisation," *IET Radar, Sonar Navigat.*, vol. 11, no. 8, pp. 1235–1242, Apr. 2017.
[16] M. Mussetta, P. Pirinoli, S. Selleri, and R. E. Zich, "Multi-objective Meta-PSO techniques for optimization of antenna arrays," in *Proc. 3rd Eur. Conf. Antennas Propag.*, Mar. 2009, pp. 503–505.
[17] G. Lu and Z. Cao, "Radiation pattern synthesis with improved high dimension PSO," in *Proc. Prog. Electromagn. Res. Symp.-Fall (PIERS-FALL)*, Nov. 2017, pp. 2160–2165.
[18] O. M. Bucci, L. Caccavale, and T. Isernia, "Optimal far-field focusing of uniformly spaced arrays subject to arbitrary upper bounds in nontarget directions," *IEEE Trans. Antennas Propag.*, vol. 50, no. 11, pp. 1539–1554, Nov. 2002.
[19] T. Isernia and A. F. Morabito, "Mask-constrained power synthesis of linear arrays with even excitations," *IEEE Trans. Antennas Propag.*, vol. 64, no. 7, pp. 3212–3217, Jul. 2016.
[20] P. Demarcke, H. Rogier, R. Goossens, and P. D. Jaeger, "Beamforming in the presence of mutual coupling based on constrained particle swarm optimization," *IEEE Trans. Antennas Propag.*, vol. 57, no. 6, pp. 1655–1666, Jun. 2009.
[21] A. Pirhadi, M. Rahmani, and A. Mallahzadeh, "Shaped beam array synthesis using particle swarm optimisation method with mutual coupling compensation and wideband feeding network," *IEE Microw., Antennas, Propag.*, vol. 8, no. 8, pp. 549–555, 2014.
[22] T. Macnamara, *Introduction to Antenna Placement and Installation*. Hoboken, NJ, USA: Wiley, 2010.
[23] B. Zhang and Y. Rahmat-Samii, "Robust optimization with worst case sensitivity analysis applied to array synthesis and antenna designs," *IEEE Trans. Antennas Propag.*, vol. 66, no. 1, pp. 160–171, Jan. 2018.
[24] O. P. Acharya and A. Patnaik, "Antenna array failure correction [antenna applications corner]," *IEEE Antennas Propag. Mag.*, vol. 59, no. 6, pp. 106–115, Dec. 2017.
[25] W. C. Weng, F. Yang, and A. Z. Elsherbeni, "Linear antenna array synthesis using Taguchi's method: A novel optimization technique in electromagnetics," *IEEE Trans. Antennas Propag.*, vol. 55, no. 3, pp. 723–730, Mar. 2007.
[26] W. C. Weng, F. Yang, and A. Z. Elsherbeni, "Integration of taguchi's method and particle swarm optimization for electromagnetic global optimization," in *Proc. 2nd Eur. Conf. Antennas Propag. (EuCAP)*, Nov. 2007, pp. 1–6.
[27] X.-S. Yang, "Firefly algorithms for multimodal optimization," in *Stochastic Algorithms: Foundations and Applications* (Lecture Notes in Computer Science), vol. 5792, O. Watanabe and T. Zeugmann, Eds. Berlin, Germany: Springer, 2009.
[28] A. Winterstein and A. Dreher, "A hybrid self-tracking receiver implementation with direction-of-arrival estimation for retro-directive antenna systems," *IEEE Trans. Microw. Theory Techn.*, vol. 65, no. 12, pp. 5422–5431, Dec. 2017.
[29] D. L. Lemes, M. V. T. Heckler, and A. Winterstein, "A low-cost modular transmit front-end with analog beamforming capability," in *IEEE MTT-S Int. Microw. Symp. Dig.*, Aug. 2017, pp. 1–5.

LUKASZ A. GREDA (M'01–SM'17) received the Dipl.Ing. (M.S.) degree in electrical engineering from the Kielce University of Technology, Poland, in 1999, and the Dr. Ing. (Ph.D.) degree in electrical engineering from FernUniversität, Hagen, Germany, in 2005.

From 1999 to 2004, he was a Research Assistant with the Department of Electrical Engineering, FernUniversität. Since 2004, he has been with the Antenna Research Group, Institute of Communications and Navigation, German Aerospace Center (DLR), Oberpfaffenhofen, Germany, as a Senior Research Associate. His current research interests include analysis of microstrip antennas, smart antennas, and antenna technology for satellite communications and navigation.

ANDREAS WINTERSTEIN (M'12) received the Dipl.Ing. (M.Sc.) degree from Technische Universität Darmstadt, Germany, in 2011, and the Dr. Ing. (Ph.D.) degree in retro-directive antenna systems from the Technical University of Munich, Germany, in 2019. He joined the Antenna Research Group, Institute of Communications and Navigation, German Aerospace Center (DLR), Oberpfaffenhofen. His current research interests include hybrid digital/analog retro-directive antenna systems and robust navigation receivers.

DANIEL L. LEMES was born in Paracatu, Brazil, in 1990. He received the B.Sc. and M.Sc. degrees in electrical engineering from the Universidade Federal do Pampa (UNIPAMPA), Alegrete, Brazil, in 2015 and 2018, respectively, He is currently pursuing the Ph.D. degree with the Universidade Federal de Santa Maria (UFSM), Santa Maria, Brazil.

MARCOS V. T. HECKLER (M'06) was born in Rio Grande, Brazil, in 1978. He received the B.Sc. degree in electrical engineering (with an emphasis on electronics) from the Universidade Federal de Santa Maria (UFSM), Santa Maria, Brazil, in 2001, the M.Sc. degree in electronic engineering (microwaves and optoelectronics) from the Instituto Tecnológico de Aeronáutica (ITA), São José dos Campos, Brazil, in 2003, and the Dr. Ing. degree in electrical engineering from the Technische Universität München, Munich, Germany, in 2010.

From April to August 2003, he was a Research Assistant with the Antennas and Propagation Laboratory, ITA. From October 2003 to June 2010, he was a Research Associate with the Antenna Group, Institute of Communications and Navigation, German Aerospace Center (DLR). He is currently a Professor with the Universidade Federal do Pampa, Alegrete, Brazil, where he is also the Head of the Electromagnetics, Microwaves and Antennas Laboratory. His current research interests include the design of microstrip antennas and arrays, and the development of numerical techniques for microstrip antennas.